Chemical Physics Letters 739 (2020) 137034

Contents lists available at ScienceDirect

Chemical Physics Letters

journal homepage: www.elsevier.com/locate/cplett

Research paper

Orientation dependence of phase memory relaxation in the V(IV) ion at high frequencies

Cassidy E. Jackson[a], Chun-Yi Lin[a], Johan van Tol[b], Joseph M. Zadrozny[a,*]

[a] Department of Chemistry, Colorado State University, 1301 Center Ave., Fort Collins, CO 80523-1872, United States
[b] National High Magnetic Field Laboratory, 1800 E. Paul Dirac Dr., Tallahassee, FL 32310, United States

HIGHLIGHTS

- Canonical orientations of magnetic complexes in a magnetic field produce longer phase memory relaxation times.
- V(IV) phase memory relaxation hastens at high magnetic fields (> 4 T).
- V(IV) spin lattice relaxation hastens at high field (> 4 T).
- Deuteration at high field slows phase memory relaxation for V(IV) by a factor of 1.5.

ARTICLE INFO

Keywords:
Phase memory relaxation
Coordination complexes
Pulsed electron paramagnetic resonance

ABSTRACT

Understanding how magnetic relaxation depends on molecular orientation is a fundamental parameter for designing magnetic molecules for application. Herein we report the first use of pulsed high-frequency electron paramagnetic resonance spectroscopy (HFEPR, 120 and 240 GHz) to define the orientation dependence of phase memory relaxation in the $S = {}^1/_2$ V(IV) complex $(n\text{-Bu}_3\text{NH})_2[\text{V}(\text{C}_6\text{H}_4\text{O}_2)_3]$. We demonstrate a variation of 20% of the phase memory relaxation time (T_m) as a function of the orientation of the $[\text{V}(\text{C}_6\text{H}_4\text{O}_2)_3]^{2-}$ molecule in the applied magnetic field. Ultimately, this work underlines an important design strategy for molecule-based quantum computing architectures.

1. Introduction

Molecular qubits are a potential centrepiece in next-stage quantum information processing and sensing schemes [1–4]. Indeed, spin-based superpositions in molecules can be engineered via synthetic design to be exceedingly stable as indicated by phase-memory relaxation times (T_m) on millisecond timescales [5,6]. Prominent proposals for building actual molecule-scale quantum computers to seize upon these discoveries are predominantly surface-based [7–10]. Here, qubits are oriented in precise arrays to encourage entanglement and individual manipulation, effectively generating small test-scale spin-based quantum computing devices. Toward this goal, understanding molecular qubit properties upon surface deposition is essential [7–13].

One important piece of that information pertains to the orientation of the molecule on the surface. Designing surface-based molecular computers hinges on knowing precisely how magnetic orientation affects properties. Indeed, many recent proposals feature specific surface orientations of metal ions [14,15], or structurally anisotropic metal complexes that could be readily envisioned to align on surfaces [6,11,12,16]. Yet, orientation-dependent studies of spin-based properties are relatively rare in the present explosion of interest in metal-ion molecular qubits, despite their necessity in identifying the optimal orientations to target.

In this manuscript, we use high-field/high-frequency (120 and 240 GHz) electron paramagnetic resonance (HFEPR) for the first time to define how molecular orientation affects T_m in the candidate molecular qubit $(n\text{-Bu}_3\text{NH})_2[\text{V}(\text{C}_6\text{H}_4\text{O}_2)_3]$ (**1**) (Fig. 1) [17]. HFEPR enables the high resolution of resonances from molecules at specific alignments in magnetic field (when g_z, g_x, and g_y are coincident with B_0) [18]. This resolution is higher than typically possible at the frequencies of conventional EPR (X-band, ca. 3500 G), wherein other magnetic interactions (e.g. hyperfine coupling or zero-field splitting) engender overlapping peaks. Hence, HFEPR is indispensable for orientation-dependent investigations of T_m. Furthermore, high fields enhance spin polarization [19,20], facilitate qubit initialization [21], suppress environmental magnetic noise [22], and are typical for dynamic nuclear

* Corresponding author.
E-mail address: joe.zadrozny@colostate.edu (J.M. Zadrozny).

https://doi.org/10.1016/j.cplett.2019.137034
Received 16 November 2019; Received in revised form 9 December 2019; Accepted 11 December 2019
Available online 12 December 2019
0009-2614/

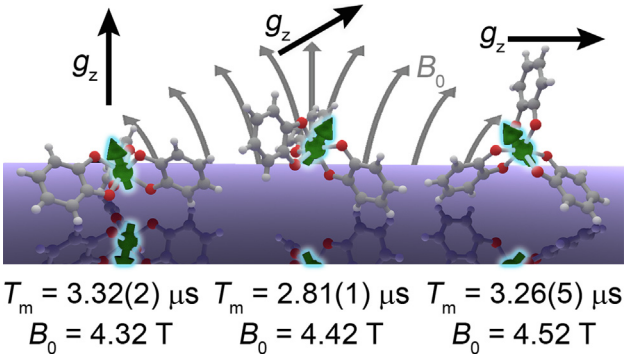

Fig. 1. Graphical depiction of orientation dependence of phase memory relaxation in $[V(C_6H_4O_2)_3]^{2-}$ relative to B_0. Selected T_m values are shown under select orientations of **1**, as determined from frozen-solution spectra.

polarization (DNP) [23,24]. These points underscore the broader importance of using the technique to understand the high-field magnetic properties of molecular qubits, particularly containing metal ions.

We focus on the extremely promising V(IV) ion – molecular qubits of V(IV) enable synthetic control, long-lived phase memory relaxation (T_m), and long spin-lattice relaxation times (T_1) in select species, e.g. $[V(C_8S_8)_3]^{2-}$ [5,6,25-30]. Yet, to the best of our knowledge, only one previous report of the coherent spin dynamics of V(IV) properties at high field exists [29]. Hence, the impact of both the chemical environment and molecular orientation on V(IV) electron spin coherence at high field remains untested – critical information to design future qubits using this ion. Herein, we use **1** for an initial test of orientation dependence at high field, not because of a unique or large T_m, but because of the well-studied nature of its low-field relaxation and, hence, facility of comparison with the present high-field conditions [26,29,30]. These studies demonstrate a smaller T_m-dependence on solvent deuteration at high field for the V(IV) ion (relative to low field). Furthermore, we demonstrate a significant change in T_m (ca. 20%) as a function of orientation. Importantly, our results reveal the highest T_m for canonical orientations (Fig. 1). These results, the first of which for a V(IV) complex at high field and frequency, support many of the recent surface-based proposals for highly oriented molecules in spin-based quantum computing architectures [10,15].

2. Experimental

2.1. General considerations

The complex $(n\text{-}Bu_3NH)_2[V(C_6H_4O_2)_3]$ (**1**) was reported to be air-sensitive [30]. Thus, all manipulations and syntheses of it were performed under a N_2 atmosphere with either a Vigor glovebox or Schlenk techniques. Both *o*-terphenyl (98%, Alfa Aesar) and d^{14}-*o*-terphenyl (98% ^2H, Cambridge Isotope Laboratories) were used as received. The complex $(n\text{-}Bu_3NH)_2[V(C_6H_4O_2)_3]$ (**1**) was prepared following the literature procedures [30].

2.2. Electron paramagnetic resonance measurements

EPR spectra collected herein were simulated using Easyspin [31] with the function pepper (frozen solution and solid) and were refined using simulations of the experimental data. All samples were prepared under an inert atmosphere of N_2. Sample **1** for pulsed EPR studies (1 mM) were prepared by first loading 20 μL 1 mM THF solution of **1** by a micropipette into a 4 mm OD quartz EPR tube. Following removal of THF under reduced pressure, 0.0232 g o-terphenyl or 0.0258 g deuterated o-terphenyl (20 μL when molten) was loaded into the same tube. These tubes were flame sealed under dynamic vacuum (< 50 mTorr) and placed in a 65–70 °C oil bath until a clear dark blue solution formed. Sample tubes prepared in this manner can be stored at room temperature for an extended period without compound decomposition, but the OTP will slowly crystallize. Hence, prior to each measurement, the samples were remelted and refrozen to produce a high-quality glass.

All pulsed EPR data were collected at the National High Magnetic Field Laboratory (NHMFL, Tallahassee, FL, USA) on a custom built 120/240/336 GHz EPR spectrometer [32,33]. Sample tubes were gently melted using a heat gun to afford a homogeneous dark blue solution, then quickly inserted into the cold same chamber to ensure glass formation. The collected data were processed using an EPR measurement program locally developed at NHMFL, Matlab 2018b, and Origin Pro 2018b software packages [34,35].

T_1 data were collected on the most intense resonance of the EDFS spectra at 4.4 T at 120 GHz, via an inversion recovery sequence (π–*T*–π/2–τ–π–τ–echo). The length of the three pulses, π–π/2–π, are 900–600–900 ns with a starting *T* value of 10300 ns and τ of 700 ns. The inversion recovery data were fit accounting for spectral diffusion with the following equation:

$$I(t) = -A\left[e^{\left(-\frac{t}{T_1}+\sqrt{\frac{t}{q}}\right)} - I(0) - 1\right]$$

Here, *A* is a preexponential factor, T_1 is the spin lattice relaxation time, *t* is the delay following the inversion pulse, *q* is a parameter specifically related to the presence of spectral diffusion [36], and *I*(0) is the intensity at zero delay. Variable-temperature T_1 data presented challenges in fitting due to the enhanced relaxation rate of spin-lattice relaxation with 120 GHz frequencies. As a result, measurements were restricted to below 40 K.

T_m data for 120 GHz were collected on the most intense resonance (4.4 T at 120 GHz) in the EDFS spectra via a Hahn echo sequence (π/2–τ–π–τ–echo) with a 4-step phase cycle with microwave pulses of 600 (π/2) and 900 ns (π) and a starting interpulse delay (τ) of 700 ns. T_m data for 240 GHz were collected on the most intense resonance (8.8 T at 120 GHz) in the EDFS spectra via a Hahn echo sequence (π/2–τ–π–τ–echo) with a 4-step phase cycle with microwave pulses of 1000 (π/2) and 1200 ns (π) and a starting interpulse time (τ) of 800 ns. The Hahn echo decay data were fit using the stretched exponential equation:

$$I(\tau) = I(0) - Ae^{\left(\frac{2\tau}{T_m}\right)^{\beta}}$$

Here, *I*(0) is the echo intensity at τ = 0, *A* is a preexponential factor, τ is the interpulse delay time, T_m is the phase memory relaxation time, and *β* is the stretch parameter. The low temperature data were better fit with this stretched exponential equation as opposed to a simple monoexponential decay. Indeed, we found that β approached 1 as the temperature increased for our samples, indicating that a conventional single exponential fit could be used. Nevertheless, we used the stretched exponential fit throughout the whole temperature range for consistency.

Owing to the long pulse lengths and 100 ns deadtime, T_m values below 200–300 ns were in general extremely difficult to observe, requiring prohibitively long data acquisition times. This factor limited the temperature range for a usable echo to only the lowest temperatures, hence all analyses generally stopped by 40 K.

3. Results and discussion

Echo-detected, field-swept (EDFS) EPR spectra of $(n\text{-}Bu_3NH)_2[V(C_6H_4O_2)_3]$ (**1**) (Fig. 2, Tables S1, S2) reveal a singular broad peak using 120 and 240 GHz frequencies. As previously shown, these spectra are extremely wide compared to the sharp eight-line spectrum at X-band, likely attributable to g-strain [29]. Simulation of the spectra are nevertheless possible with the rhombic *g* (g_x = 1.941, g_y = 1.925, and g_z = 1.992) and *A* values (A_x = 313, A_y = 363, and A_z = 60 MHz) (Tables S1 and S2) [29,30]. While broad, the spectral signals

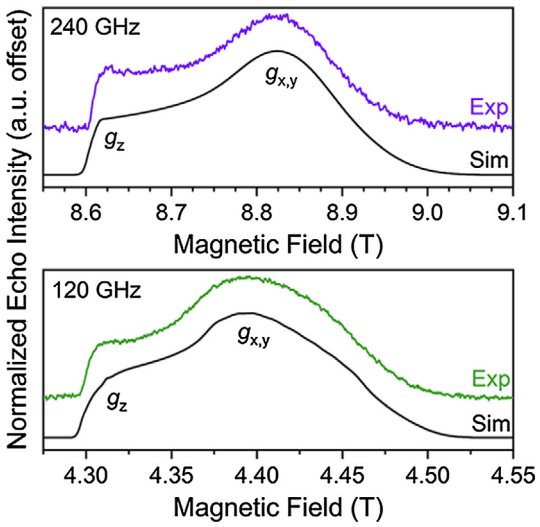

Fig. 2. Echo-detected, field-swept (EDFS) EPR spectra collected with 120 and 240 GHz microwave radiation at 4 and 4.5 K, respectively. Samples were 1 mM in frozen OTP glass. Coloured lines are experimental data, black lines are simulations for a rhombic system with $g_z > g_x > g_y$, and $A_z < A_x < A_y$ (see main text). The spectra appear nearly axial at these frequencies because of the broadening and overlap of the g_x and g_y orientations (See Fig. S1).

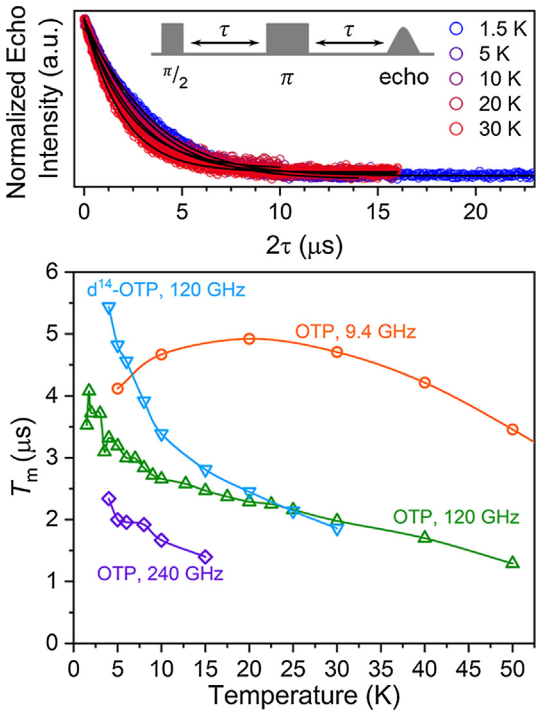

Fig. 3. (Top) Selected Hahn-echo decay curves (coloured circles) and exponential fit (black trace) for **1** in OTP at 120 GHz. **(Bottom)** Variable-temperature T_m data at 9.4, 120, and 240 GHz for **1** in OTP or d^{14}-OTP glass. The 9.4 GHz data were taken from refs. 28–30. Error bars are within the width of the data points.

nevertheless contain important, resolvable features – the sharp, low-field feature results from molecules with g_z aligned to the magnetic field (B_0), while the more intense, high-field feature stems from molecules where $g_{x,y}$ is parallel to B_0 (Fig. S1). In contrast, at X-band frequencies ($B_0 \sim 3400$ G), the signals from these three orientations are entirely overlaid [30]. As one final point – the broadness of the spectra at high frequency precluded precise resolution of hyperfine coupling, hence, the values of A used were from earlier publication [28,29].

Preliminary evaluation of the spin dynamics of **1** proceeded by analysis of the spin–lattice relaxation times using inversion recovery experiments at the strongest-intensity peak in the EDFS. These experiments were performed at 120 GHz for **1** dissolved to 1 mM concentration in protiated and deuterated *o*-terphenyl (OTP). The values of T_1 are essentially the same between the two matrices (Figs. S2 and S3, Tables S3, S4), demonstrating that environmental deuteration impacts T_1 negligibly at these frequencies.

Next, we investigated the temperature and matrix dependence of phase memory time, or T_m. Here, we performed two-pulse Hahn echo experiments at the strongest peak in the EDFS as a function of temperature (Figs. 3, S4, S5) to extract T_m in OTP and d^{14}-OTP. At 120 GHz and 5 K, T_m of **1** in d^{14}-OTP is 4.82(3) μs and is temperature dependent in the regime measured. When compared to the T_m of **1** in OTP at 120 GHz and 5 K, T_m is shorter with a value of 3.192(9) μs. With increasing temperature T_m drops, reaching the same T_m as **1** in OTP by 25 K. In comparison to both 120 GHz data sets, T_m of **1** in OTP at 240 GHz is relatively much shorter, with a T_m of 2.00(5) μs at 5 K, dropping to 1.40(4) μs at 15 K. When compared to T_m collected at X-band frequency in OTP, we notice a similar T_m of 4.12(3) μs at 5 K, yet T_m here is not as temperature-dependent (Fig. 3) [30]. Note that these data were successfully fit without a noticeable stretch parameter, implying that methyl group rotation on the counterion is not a governing factor in T_m here (Tables S5, S6).

The temperature and matrix dependence of T_m highlights the environmental role in controlling phase memory relaxation. The use of a deuterated solvent typically increases T_m by a factor of about two or more in metal complexes [5,37,38], due to the lower nuclear magnetic dipole moment of deuterium (0.86 μ_N) relative to the proton (2.79 μ_N) [39,40]. Yet, we observe a slightly smaller enhancement, by a factor of 1.5. This relatively smaller enhancement factor may suggest that other mechanisms of decoherence are operative at high frequency (rather than common interactions with the nuclear spin bath). Indeed, the T_m of the probed spins is strongly temperature dependent in the studied window, potentially highlighting the impact of a shorter, temperature-dependent T_1 from other V(IV) spins in the sample [41]. However, another factor may be the relatively small density of nuclear spins in OTP (45 ^{1}H/nm^3) versus other solvents (e.g H_2O, 66 ^{1}H/nm^3). Furthermore, we do not detect a low temperature downturn of T_m of **1** as was seen when rotation of –CH_3 groups on the *n*-Bu_3NH^+ counterions directed T_m at X-band [30]. Finally, T_m decreases from 120 to 240 GHz in the same sample, in trend with the expected field dependence of T_1 for this ion [29].

The nearly 0.3 T separation of signals from $[V(C_6H_4O_2)_3]^{2-}$ molecules with g_z oriented parallel and perpendicular to the magnetic field suggested that HFEPR would be ideal for testing the orientation dependence of T_m. This prospect is especially tantalizing relative to conventional X-band EPR, where peaks corresponding to different orientations are extremely close (~0.01 T) and overlap. Since **1** is approximately axial, we hypothesized that T_m would be longer where g_z for $[V(C_6H_4O_2)_3]^{2-}$ is parallel or perpendicular to B_0. Indeed, simulations of the resonant field (B) as a function of angle between g_z and B_0 (θ) suggested a stable EPR frequency to small motions at these alignments (i.e. $\Delta B/\Delta\theta$ is small, Fig. 4). As small changes in resonant frequency induce relaxation, orientations where $\Delta B/\Delta\theta$ is small (here, where g_z, g_x, and g_y are parallel to B_0) might therefore exhibit the highest T_m – providing a clear design principle for surface attachment of molecular qubits.

To test this hypothesis, we evaluated T_m via Hahn-echo experiments as a function of magnetic field at 120 and 240 GHz (Figs. 4, S6, Tables S7, S8). At 120 GHz and 5 K in OTP, we see T_m reach a maximum of 3.32(2) μs at 4.32 T (where g_z for the molecule is coincident with B_0), then drop with increasing field, reaching 2.73(1) μs at 4.46 T, before climbing to 3.26(5) μs at 4.52 T (where g_x, g_y are coincident and g_z is perpendicular to B_0). Overall, the variation in T_m is about 20% as a function of orientation. At 240 GHz and 5 K, also in OTP, similar

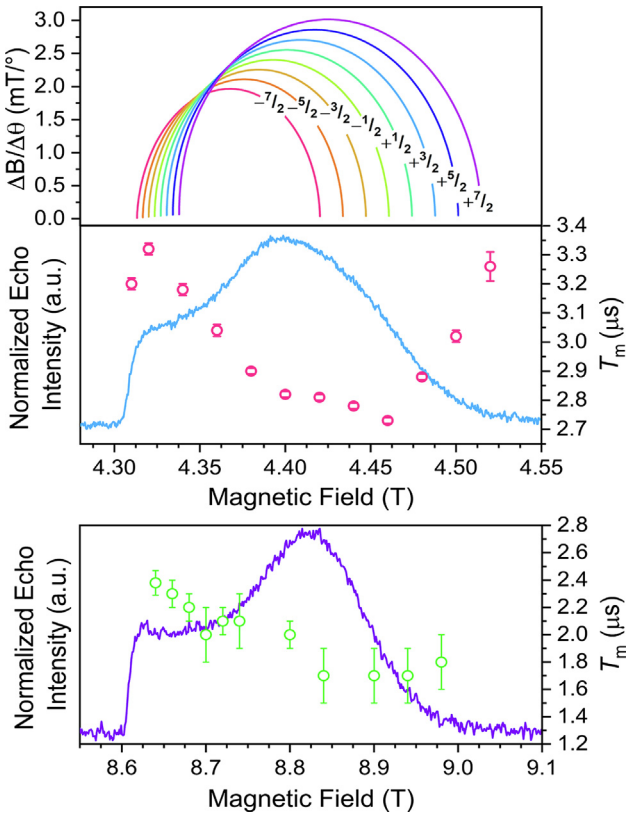

Fig. 4. (Top) Change in the resonant field (B) with respect to orientation as a function of background applied magnetic field for each of the transitions in the 120 GHz EDFS. Transitions are labeled with their corresponding M_I value. The $\Delta B/\Delta_\theta$ values were calculated using microwave frequency = 120 GHz and *g*- and *A*-parameters listed in Table S1. **(Middle)** EDFS and orientation dependence of T_m for **1** at 120 GHz and 4 K. The fields for the top/middle panels aligned for ease of comparison. **(Bottom)** EDFS and orientation dependence of T_m for **1** at 240 GHz and 4.5 K. All measurements here were in OTP.

behaviour is seen, wherein T_m is 2.38(9) μs at 8.64 T, drops with increasing field, then climbs again to 1.8(2) μs at 8.98 T (Fig. S6). These results demonstrate a smaller variation in T_m as a function of orientation than the 41% observed for **1** at X-band frequency [30]. Although modest, the orientation-dependent data nevertheless shows how specific orientations of molecular species can enhance T_m.

Our results show that T_m is longer along the edges of the EDFS spectrum, when g_x and g_y, or g_z are coincident to B_0. This observation is consistent with a scenario where slight changes in molecular geometry (via librations) dictate only small changes in resonant field ($\Delta B/\Delta\theta$ is $\approx$ 0), as is well-established [42,43]. The results of the small $\Delta B/\Delta\theta$ are emphasized at 4.32 T and 4.52 T in the 120 GHz data, where there is likely only one hyperfine transition being probed (Fig. 4). This observation of high T_m only at the spectral extrema likely stems from the inability to resolve the individual hyperfine peaks relative to the X-band data. Hence, the only places in the EDFS spectrum where most of the spins exhibit a small $\Delta B/\Delta\theta$ are the edges of the spectrum. This aspect is in contrast to the X-band data where the longest T_ms occur in the middle of the EDFS spectrum owing to highly overlapping peaks at 120 GHz.

Reported orientation dependence studies of metal complexes are largely limited to X-band frequencies. For example, other groups report large variations (> 40%) of T_m at X-band for vanadyl [44], Cu(II) [44–46], Mo(V) [47], and Cr(V) [48] systems. The relatively lower variation observed in this study may stem from the use of a higher magnetic fields, which are likely changing the dominant relaxation processes in **1**. One possibility for the weaker orientation dependence is that T_m is being shortened via the decreased T_1 for $[V(C_6H_4O_2)_3]^{2-}$ at high frequency. However, even though the recorded high frequency T_1 for **1** is shorter at 120 GHz (~1 ms), it is still ~3 orders of magnitude higher than T_m at the temperature of the orientation dependence studies (5 K), suggesting that spin-lattice relaxation is not the dominant mechanism of phase memory relaxation. Other studies suggest that librations may play a more prominent role at high frequency in shortening T_m [49]. Ultimately, future studies are required to truly understand the mechanisms responsible for magnetic relaxation in **1** at high frequency.

4. Conclusions and outlook

The foregoing results constitute the first orientation-dependent study of T_m in V(IV) using pulsed, high-frequency EPR. Importantly, we observe a 20% variation in T_m as a function of magnetic field, with peak T_m values when g_z is parallel and perpendicular to B_0. Hence, these data underline an orientation-driven design principle for addressing the challenge of scaling in spin-qubit processors. We note that these results were obtained by studying frozen glass solutions, not surface-mounted molecules, and the molecular dynamics should be significantly different in the latter scenario. Hence, additional studies of molecules on surfaces will ultimately be needed to evaluate whether the orientation dependence observed here translates to surface-based architectures. Finally, to the extent that these results can assist in targeting higher T_m in potential qubits at these high fields, studies of other ions with varying *g*-anisotropy or higher T_1 at these fields (e.g. VO^{2+} or Cu^{2+}) may pave the way to the desired insight. These studies will be reported in due course.

CRediT authorship contribution statement

Cassidy E. Jackson: Conceptualization, Investigation, Writing - original draft, Writing - review & editing. **Chun-Yi Lin:** Conceptualization, Investigation, Writing - review & editing. **Johan van Tol:** Investigation, Writing - review & editing. **Joseph M. Zadrozny:** Conceptualization, Writing - original draft, Writing - review & editing.

Declaration of Competing Interest

The authors declare that they have no known competing financial interests or personal relationships that could have appeared to influence the work reported in this paper.

Acknowledgements

We acknowledge support from Colorado State University and the National Science Foundation (CHE-1836537). A portion of this work was performed at the National High Magnetic Field Laboratory, which is supported by the National Science Foundation through NSF/DMR-1157490/1644779 and the State of Florida.

Appendix A. Supplementary material

Supplementary data to this article can be found online at https://doi.org/10.1016/j.cplett.2019.137034.

References

[1] M. Atzori, R. Sessoli, J. Am. Chem. Soc. 141 (2019) 11339–11352.
[2] M. Affronte, F. Troiani, A. Ghirri, A. Candini, M. Evangelisti, V. Corradini, S. Carretta, P. Santini, G. Amoretti, F. Tuna, G. Timco, R.E.P. Winpenny, J. Phys. D: Appl. Phys 40 (2007) 2999–3004.
[3] A. Gaita-Ariño, F. Luis, S. Hill, E. Coronado, Nat. Chem. 11 (2019) 301–309.
[4] M.J. Graham, J.M. Zadrozny, M.S. Fataftah, D.E. Freedman, Chem. Mater. 29 (2017) 1885–1897.

[5] J.M. Zadrozny, J. Niklas, O.G. Poluektov, D.E. Freedman, ACS Cent. Sci. 1 (2015) 488–492.
[6] C.-J. Yu, M.J. Graham, J.M. Zadrozny, J. Niklas, M.D. Krzyaniak, M.R. Wasielewski, O.G. Poluektov, D.E. Freedman, J. Am. Chem. Soc. 138 (2016) 14678–14685.
[7] A. Ghirri, V. Corradini, V. Bellini, R. Biagi, U. del Pennino, V. De Renzi, J.C. Cezar, C.A. Muryn, G.A. Timco, R.E.P. Winpenny, M. Affronte, ACS Nano 5 (2011) 7090–7099.
[8] Y. Bae, K. Yang, P. Willke, T. Choi, A.J. Heinrich, C.P. Lutz, Sci. Adv. 4 (2018) eaau4159.
[9] A. Hofmann, Z. Salman, M. Mannini, A. Amato, L. Malavolti, E. Morenzoni, T. Prokscha, R. Sessoli, A. Suter, ACS Nano 6 (2012) 8390–8396.
[10] D. Gatteschi, A. Cornia, M. Mannini, R. Sessoli, Inorg. Chem. 48 (2009) 3408–3419.
[11] M. Warner, S. Din, I.S. Tupitsyn, G.W. Morley, A.M. Stoneham, J.A. Gardener, Z. Wu, A.J. Fisher, S. Heutz, C.W.M. Kay, G. Aeppli, Nature 503 (2013) 504–508.
[12] L. Tesi, E. Lucaccini, I. Cimatti, M. Perfetti, M. Mannini, M. Atzori, E. Morra, M. Chiesa, A. Caneschi, L. Sorace, R. Sessoli, Chem. Sci. 7 (2016) 2074–2083.
[13] M. Mannini, F. Bertani, C. Tudisco, L. Malavolti, L. Poggini, K. Misztal, D. Menozzi, A. Motta, E. Otero, P. Ohresser, P. Sainctavit, G.G. Condorelli, E. Dalcanale, R. Sessoli, Nat. Commun. 5 (2014) 4582.
[14] L. Malavolti, M. Briganti, M. Hänze, G. Serrano, I. Cimatti, G. McMurtrie, E. Otero, P. Ohresser, F. Totti, M. Mannini, R. Sessoli, S. Loth, Nano Lett. 18 (2018) 7955–7961.
[15] M.D. Jenkins, D. Zueco, O. Roubeau, G. Aromí, J. Majer, F. Luis, Dalton Trans. 45 (2016) 16682–16693.
[16] J. McGuire, H.N. Miras, E. Richards, S. Sproules, Chem. Sci. 10 (2019) 1483–1491.
[17] S.R. Cooper, Y.B. Koh, K.N. Raymond, J. Am. Chem. Soc. 104 (1982) 5092–5102.
[18] J. van Tol, G.W. Morley, S. Takahashi, D.R. McCamey, C. Boehme, M.E. Zvanut, Appl. Magn. Reson. 36 (2009) 259–268.
[19] Molecular Nanomagnets, Oxford University Press, Oxford, New York, 2006.
[20] S.S. Eaton, G.R. Eaton, L.J. Berliner, Biomedical EPR - Part A: Free Radicals, Metals, Medicine and Physiology, Springer Science & Business Media, 2004.
[21] D.P. Vincenzo, Fortschr. Phys. 48 (2000) 771–783.
[22] S. Takahashi, R. Hanson, J. Van Tol, M.S. Sherwin, D.D. Awschalom, Phys. Rev. Lett. 101 (2008) 1–4.
[23] M.D. Lingwood, S. Han, Annu. Rep. NMR Spectrosc. 73 (2011) 83–126.
[24] T. Maly, G.T. Debelouchina, V.S. Bajaj, K.-N. Hu, C.-G. Joo, M.L. Mak-Jurkauskas, J.R. Sirigiri, P.C.A. van der Wel, J. Herzfeld, R.J. Temkin, R.G. Griffin, J. Chem. Phys. 128 (2008) 052211.
[25] M.S. Fataftah, M.D. Krzyaniak, B. Vlaisavljevich, M.R. Wasielewski, J.M. Zadrozny, D.E. Freedman, Chem. Sci. 10 (2019) 6707–6714.
[26] M. Atzori, S. Benci, E. Morra, L. Tesi, M. Chiesa, R. Torre, L. Sorace, R. Sessoli, Inorg. Chem. 57 (2018) 731–740.
[27] M. Atzori, L. Tesi, S. Benci, A. Lunghi, R. Righini, A. Taschin, R. Torre, L. Sorace, R. Sessoli, J. Am. Chem. Soc. 139 (2017) 4338–4341.
[28] M. Atzori, E. Morra, L. Tesi, A. Albino, M. Chiesa, L. Sorace, R. Sessoli, J. Am. Chem. Soc. 138 (2016) 11234–11244.
[29] C.E. Jackson, C.-Y. Lin, S.H. Johnson, J. van Tol, J.M. Zadrozny, Chem. Sci. 10 (2019) 8447–8454.
[30] C.-Y. Lin, T. Ngendahimana, G.R. Eaton, S.S. Eaton, J.M. Zadrozny, Chem. Sci. 10 (2019) 548–555.
[31] S. Stoll, A. Schweiger, J. Magn. Reson. 178 (2006) 42–55.
[32] J. van Tol, L.-C. Brunel, R.J. Wylde, Rev. Sci. Instrum. 76 (2005) 074101.
[33] G.W. Morley, L.-C. Brunel, J. van Tol, Rev. Sci. Instrum. 79 (2008) 064703.
[34] Matlab; The MathWorks Inc.: Natick, MA, 2018.
[35] Origin; OriginLab: Northampton, MA, 2018.
[36] H. Chen, A.G. Maryasov, O.Y. Rogozhnikova, D.V. Trukhin, V.M. Tormyshev, M.K. Bowman, Phys. Chem. Chem. Phys. 18 (2016) 24954–24965.
[37] J.M. Zadrozny, D.E. Freedman, Inorg. Chem. 54 (2015) 12027–12031.
[38] K. Bader, M. Winkler, J. van Slageren, Chem. Comm. 52 (2016) 3623–3626.
[39] W.M. Haynes, T.J. Bruno, D.R. Lide, CRC Handbook of Chemistry and Physics: A Ready-reference Book of Chemical and Physical Data, CRC Press, 2014.
[40] N.J. Stone, At. Data Nucl. Data Tables 32 (2005) 75–176.
[41] K.M. Salikhov, S.A. Dzuba, A.M. Raitsimring, J. Magn. Reson. 42 (1981) 255–276.
[42] M. Rohrer, P. Gast, K. Möbius, T.F. Prisner, Chem. Phys. Lett. 259 (1996) 523–530.
[43] S.A. Dzuba, Phys. Lett. A 213 (1996) 77–84.
[44] J.-L. Du, K.M. More, S.S. Eaton, G.R. Eaton, Isr. J. Chem. 32 (1992) 351–355.
[45] J.-L. Du, G.R. Eaton, S.S. Eaton, J. Magn. Reson. Ser. A 117 (1995) 67–72.
[46] A.J. Fielding, S. Fox, G.L. Millhauser, M. Chattopadhyay, P.M.H. Kroneck, G. Fritz, G.R. Eaton, S.S. Eaton, J. Magn. Reson. 179 (2006) 92–104.
[47] R. Husted, J.-L. Du, G.R. Eaton, S.S. Eaton, Magn. Reson. Chem. 33 (1995) S66–S69.
[48] R. Konda, J.-L. Du, S.S. Eaton, G.R. Eaton, Appl. Magn. Reson. 7 (1994) 185–193.
[49] S.K. Misra, Multifrequency Electron Paramagnetic Resonance, Wiley-VCH Verlag GmbH & Co. KGaA, Weinheim, 2011.